PCCP

Accepted Manuscript

ROYAL SOCIETY OF CHEMISTRY

www.rsc.org/pccp

PCCP

ARTICLE

Monitoring a CuO gas sensor at work: an advanced *in situ* X-ray absorption spectroscopy study†

Received 00th January 20xx,
Accepted 00th January 20xx

DOI: 10.1039/x0xx00000x

www.rsc.org/

D. P. Volanti,[a,b] A. A. Felix,[b] P. H. Suman,[b] E. Longo,[b] J. A. Varela,[b] M. O. Orlandi[b,*]

X-ray absorption near edge structure (XANES) and electrical measurements were used to elucidate the local structure and electronic changes of copper (II) oxide (CuO) nanostructures under working conditions. For this purpose, a sample holder layout was developed enabling the simultaneous analysis of the spectroscopic and electrical properties of the sensor material under identical operating conditions. The influence of the different carrier gases (e.g., air and N_2) on the CuO nanostructures behavior under reducing conditions (H_2 gas) was studied to analyze how a particular gas atmosphere can modify the oxidation state of the sensor material in real time.

1. Introduction

In the last few years, many strategies aiming to enhance the performance of metal semiconductor gas sensor materials have been reported.[1-5] P-type semiconductors have been investigated as an alternative to n-type semiconductors to enhance the gas-sensing properties of metal semiconductor gas sensor materials due to their high surface reactivity and catalytic properties.[6] Among the many p-type oxide semiconductors, copper (II) oxide (CuO) has been considered for a wide range of applications, including catalysis,[7-9] fuel cells,[10,11] and solar cells,[12,13] among others.[14-17] Recently, we have demonstrated that the engineering of hierarchical morphologies can be an effective way to improve the gas-sensing properties of pure CuO p-type oxide semiconductors due to the unique characteristics offered by these nanostructures, such as a large particle size and effective particle-particle contacts.[18] In addition, to achieve higher sensitivity and selectivity, more complex multilayered structures based on CuO functionalization have been reported as an alternative approach to facilitate the development of high-performance gas sensors.[19-21]

The development of high-performance sensor devices is deeply related to the comprehension of their functional principles and mechanisms. However, the mechanisms responsible for the gas-sensing properties of semiconductor materials are still not fully understood. To further elucidate the behavior of chemical sensors under real conditions, advanced spectroscopic techniques performed concomitantly with electrical measurements have been used to monitor the gas-sensing process in real time and *under in situ* and *in operando* conditions.[22-29] Many efforts have been made by innovative studies using synchrotron light for materials science, with a focus on energy applications,[30] electrochromic cathodes,[31] electrochemical redox processes,[32] supported catalysts,[33] and nuclear energy research.[34] In the gas-sensing field, the first studies in the literature have reported the use of synchrotron light techniques, such as X-ray absorption near edge structure (XANES) and extended X-ray absorption fine structure (EXAFS), to elucidate structural/electronic modifications and the role of noble metals in SnO_2-based gas-sensing materials under operating conditions.[35-38] These pioneer studies presented an *in situ* and *in operando* investigation using a fluorescence detection mode and electrical measurements showing that noble metals can be found in an oxidized state during the gas-sensing response. This type of measurement is very helpful and powerful because it can elucidate the physicochemical behavior of the solid when exposed to reactive environments, which is an important element in understanding and predicting a material's electrical/sensing properties.

In this work, we report an *in situ* study concomitantly using a transmission-mode XANES technique and electrical measurements aimed at correlating the local oxidation state and electrical changes in gas-sensing materials under identical operating conditions. In addition, to the best of our knowledge, this is the first study using time-resolved *in situ* XANES technique concomitantly with electrical measurements in a CuO p-type gas-sensing material and will contribute to a better understanding of the gas-sensing properties of this class of materials and the development of superior CuO-based gas sensors devices. An important factor in the investigation of CuO structures is the ability to analyze the role of copper oxidation states on conductance response and, consequently, the determination of the compound's chemical coordination state in the presence of different target gases. Information obtained by semi-quantitative and time-resolved *in situ* XANES studies in the range of seconds and a correlation with CuO's electrical behavior will be discussed using different baseline gases for the same reducing gas.

2. Experimental

2.1 XANES and Electrical Characterization

Time-resolved XANES spectra were taken at the Cu K-edge (8980 eV) in the dispersive X-ray beam line equipped with a focusing curved Si(111) monochromator operating in Bragg mode for the selection of the desired X-ray wavelength range (8900–9400

[a] *Instituto de Biociências, Letras e Ciências Exatas, UNESP - Univ Estadual Paulista, São José do Rio Preto, Depto de Química e Ciências Ambientais, 15054-000, Brazil.*
[b] *Instituto de Química, UNESP - Univ Estadual Paulista, Araraquara, Depto de Físico-Química, 14800-900, Brazil. E-mail: orlandi@iq.unesp.br*

† Electronic Supplementary Information (ESI) available: X-ray absorption near edge structure (XANES) and electrical measurements as function of temperature and Energy-dispersive X-ray spectroscopy (EDX). See DOI: 10.1039/x0xx00000x

eV). XANES spectra were collected at 10 s per scan during cyclic gas exposure, using hydrogen as target gas, under a constant total flow of 100 sccm using mass flow controllers (MKS). To achieve this, certified pre-mixed gas mixtures containing the target gases (H_2) diluted in pure dry N_2 and dry air (White Martins) were used. A *type K* thermocouple (placed in the alumina disks, see Figure 1) was used to measure the temperature *in situ*, and the tests were performed at 200 °C, 300 °C and 400 °C. The electrical measurements were carried out by monitoring changes in the electrical resistance using a stabilized high-voltage source-measure unit (Keithley, Model 237) using 100 mV with a 1 s delay by point; the data were collected concomitantly with the XANES spectra. The sample holder was placed in a sealed quartz tube in a conventional furnace to guarantee that the system was immersed in the identical conditions for temperature and gas concentration during the electrical and spectroscopic measurements.

2.2 Sample Preparation

For the electrical measurements, CuO powders were dispersed in isopropyl alcohol using an ultrasonic cleaner, and then the suspension was dripped directly onto alumina substrates with interdigitated platinum electrode arrays (100 µm Pt fingers spaced 100 µm apart), which enables excellent electrical contact and low noise measurements, as described in previous work.[18] For the spectroscopic measurements, 10 mg of CuO and 50 mg of boron nitride powders were mixed; this ratio was calculated using Hephaestus software and used to allow a high absorption edge signal. The pellets were pressed into disks of 5 mm diameter and 0.5 mm thickness by uniaxial pressure using less than 1.5 tons of force.

2.3 Quantitative Analyses

A semi-quantitative analysis by linear combination of the CuO, Cu_2O and Cu patterns and the experimental spectra was performed for each XANES spectra using Athena software in order to extract the relative fraction of each copper species present in the CuO sample. The spectra fitting were performed in the energy range from 8970 eV (pre-edge) to 9010 eV (post-edge) and due to the high correlation between the compounds used in this work the errors were estimated to be around 2-10% depending on the compound concentration.

2.4 Morphological Characterization

The *ex situ* morphological evolution of the CuO nanostructures was investigated using a JEOL model JSM-7500F electron microscope operated at an accelerating voltage of 10 kV equipped with an energy dispersive X-ray (EDX) detector (Thermo Scientific, model Noram System Six). CuO powders were analyzed as prepared, and then an annealing process was performed using the same sample exposed to pure dry nitrogen (95%) plus H_2 (5%) at 400 °C. Afterward, the same sample was exposed to synthetic dry air at 400 °C. The same gas-exposure time for hydrogen and synthetic dry air were used in the *in situ* conditions. A conventional sealed furnace and a total constant gas flow of 100 sccm were used during the annealing processes.

3. Results and Discussion

Figure 1 shows a 3D view of the sample holder designed to perform simultaneous X-ray absorption and electrical measurements under controlled atmospheres. The main goal of this sample holder layout is to provide high-resolution XANES spectra in the transmission mode and low-noise electrical measurements. As shown in the cross-cut magnified view of Figure 1, the sample holder consists of two alumina disks with concentric orifices, to allow XANES analyses, and a self-supported pellet between the disks, which is composed of a mixture of the target material and a background material (boron nitride). In this work, the target material was urchin-like CuO nanostructures synthesized by a microwave-assisted hydrothermal method, which was described in detail in our previous work.[18,39] This sample was chosen due to the huge density of nanospines on the urchin-like hierarchical structure which we believe could be suitable to be detected by XANES spectroscopy and presents a high sensitivity to reducing gases. For the electrical measurements, platinum interdigitated electrodes were prepared on the internal alumina disk, which were connected by platinum wires to the electrical connectors (see bottom view in Figure 1).

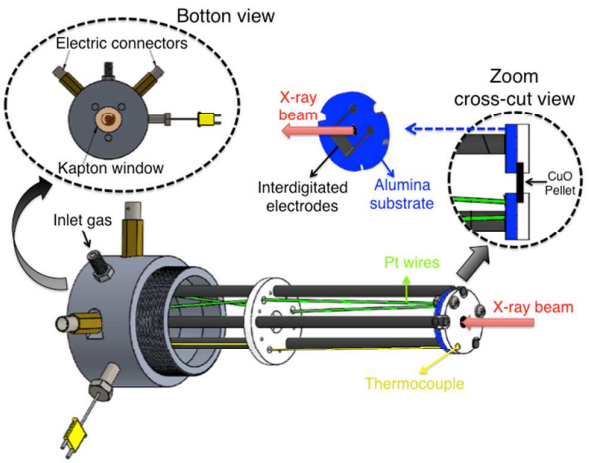

Figure 1. Sample holder layout developed to perform the *in situ* X-ray absorption measurements by transmission mode concomitantly with electrical measurements under controlled atmospheres.

Figure 2a illustrates the time-resolved *in situ* X-ray absorption in the XANES region at the Cu K-edge of the CuO nanostructures at 400 °C. Simultaneously, the electrical (gas sensor) behavior was analyzed under identical temperature and gas concentration conditions, according to the plot in Figure 2b. In this first experiment, the measurements of the CuO sample were performed under a flow of synthetic dry air as the baseline and synthetic dry air (95%) plus H_2 (5%) as the target gas. The spectra in Figure 2a indicate that CuO is present predominantly in the Cu^{2+} oxidation state with distorted octahedral coordination as the detected edge transition occurred at approximately 8994 eV during the whole cycle. The gas sensor response (Figure 2b) is typical of a p-type semiconductor exposed to reducing gases, as we have demonstrated in our previous study.[18] To further elucidate possible changes in the oxidation state of the CuO sensor during its operation, a semi-quantitative analysis based on linear combination of copper patterns and experimental data was performed to estimate the relative fraction of different

copper species (Cu^{2+}, Cu^{+} and Cu^{0}) present in the CuO sample, as shown in Figure 2c. We would like to emphasize that a linear combination is a mathematical approach, and not a modelling approach, based on fitting of the principal components on the sample to the standard compounds in which quality of the experimental spectra is very important and required. This kind of approach has been used for many researchers allowing a good correlation between experimental and theoretical interpretations.[39,40] The fitted data indicate that the CuO sample was composed of 80% (±3%) Cu^{2+} species and 20% (±10%) Cu^{+} species, which remain unchanged throughout the experiment. This high concentration of Cu^{+} species is part of the crystalline structure due to intrinsic defects, which are mainly distributed in the core of the urchin-like structure, with a small contribution resulting from the photoreduction of Cu^{2+} to Cu^{+} species caused by the X-ray beam.[39,41,42] To further evaluate the copper species present in the CuO samples, the first derivative of the XANES spectra were calculated at different times (10, 150, 1250, and 2250 s) during the sensor analysis, as shown in Figure 2d. By comparing the CuO experimental spectra with CuO, Cu_2O and Cu patterns, we can observe that the experimental spectra are very similar to the CuO spectra, corroborating the quantification data.[43,44]

The experiments were also performed at different temperatures to study the effects of temperature kinetics on the CuO gas sensor properties (see Figure S1 and S2 in ESI†). The CuO sample exhibited the same behavior at all temperatures for the X-ray absorption and electrical measurements, suggesting that no alterations in the solid composition occurred as a function of temperature when exposed to hydrogen and when using synthetic dry air as the baseline gas. These results may indicate that the changes in the resistance/conductance of CuO when exposed to reducing gases and in the presence of absorbed oxygen species at the surface are primarily related to the changes in the charge concentrations of holes/electrons near the surface.[45,46] In addition, Hübner et al. have investigated the sensing mechanism in CuO using combined DC electrical resistance and work function changes measurements demonstrating that an interaction between pre-adsorbed oxygen and water takes place at the CuO surface decreasing the concentration electronic holes because of the formation of Cu_{Cu}^{+}-OH^{-} sites at the CuO surface.[26]

Based on our results and previous reports,[18,26] we believe that in an atmosphere containing oxygen, the H_2 molecules interact with electronic holes on the CuO surface, forming H^{+} species above 150 °C (Eq. 1), and then react with preadsorbed oxygen species to form hydroxyl groups (Eq. 2 and 3) without any structural/electronic alterations to the solid compound, i.e., the hydrogen molecules induce depletion of holes at the CuO surface, resulting in increased sensor electrical resistance, as proposed by the ionosorption model and according to the following reactions:[47,48]

$$H_{2(g)} + 2h^{+} \leftrightarrow 2H^{+}_{(ads)} \quad (1)$$

$$H^{+}_{(ads)} + O_2^{-}{}_{(ads)} \leftrightarrow OH_{(ads)} + \tfrac{1}{2}\, O_{2(g)} \quad (2)$$

$$H^{+}_{(ads)} + O^{-}_{(ads)} \leftrightarrow OH_{(ads)} \quad (3)$$

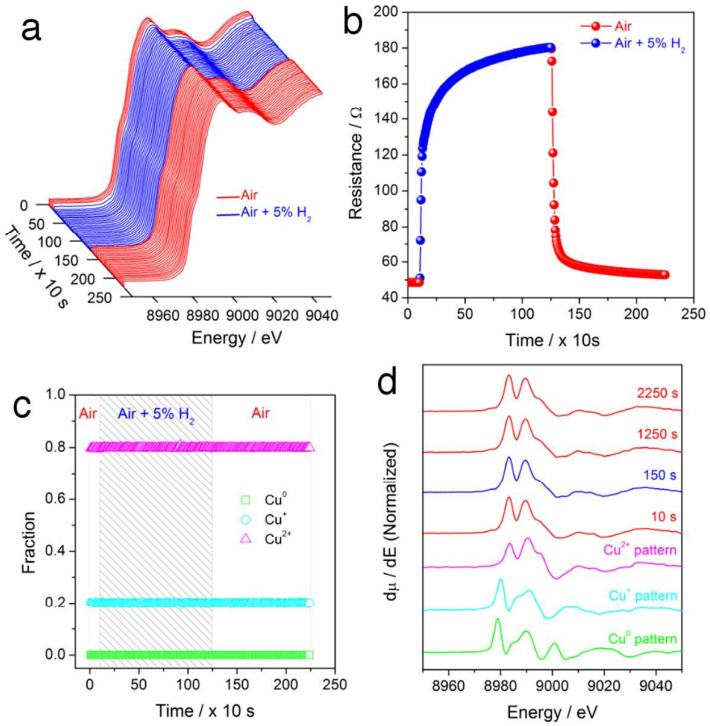

Figure 2. *In situ* measurements of urchin-like CuO nanostructures at 400 °C under cyclic exposure to synthetic dry air as the baseline and to synthetic dry air (95%) plus H_2 (5%) as the target gas. a) Time-resolved XANES spectra at the Cu K-edge; b) electrical resistance over time; c) copper fraction species over time and d) first derivative of the Cu K-edge XANES spectra at different times.

To investigate this assumption, another experiment was performed using only inert gas as a baseline and then exposing the CuO sample to hydrogen. In this experiment, the CuO sample measurements were performed under a flow of pure dry nitrogen as the baseline gas and pure dry nitrogen (95%) plus H_2 (5%) as the target gas. The results reflected abrupt changes in the XANES spectra (Figure 3a) and in the electrical resistance measurements (Figure 3b) when the CuO sample was exposed to hydrogen in the absence of oxygen. Right after the injection of hydrogen, the CuO sensor functioned as a typical p-type semiconductor by demonstrating increased electrical resistance without any changes in the XANES spectra. However, a few seconds later, the electrical resistance decreased abruptly to very low values, which are typically observed in metals, and significant alterations in the XANES spectra were observed, reflecting changes in the copper oxidation state of the CuO sample. Copper species quantification (Figure 3c) indicated the presence of Cu^0 (60±5%), Cu^+ (22±7%), and Cu^{2+} (18±10%) species after 250 s in the presence of hydrogen, compared with the initial concentration of Cu^0 (0%), Cu^+ (20±10%), and Cu^{2+} (80±3%) species under a nitrogen atmosphere. This result indicates that adsorbed hydrogen first induces the depletion of holes at the CuO surface (Eq. 1), resulting in increased sensor resistance. However, due to the absence of any oxygen species, the hydrogen reacts with the lattice oxygen, thus inducing the reduction of copper, changing the surface's solid characteristics from those of a semiconductor to those of a metal and consequently increasing sensor conductivity.

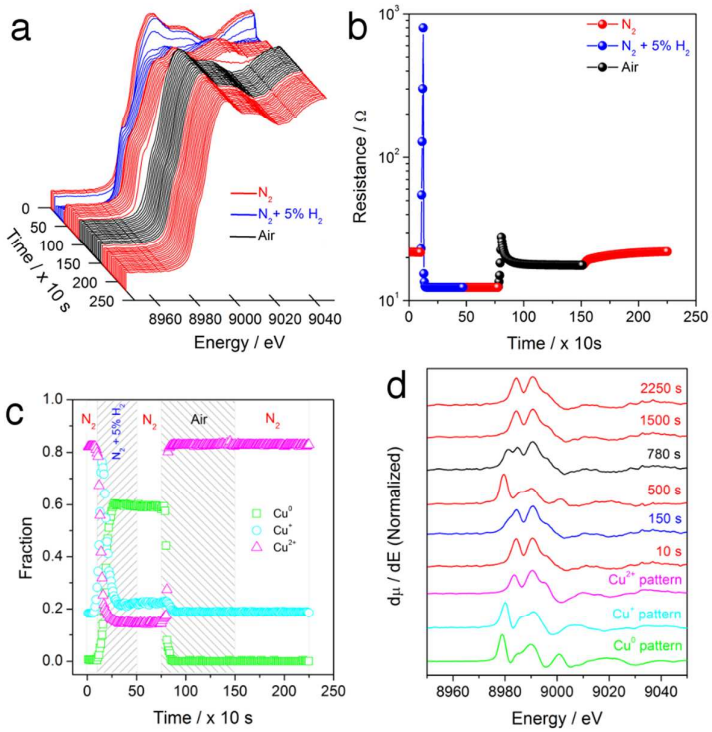

Figure 3. *In situ* measurements of urchin-like CuO nanostructures at 400 °C under cyclic exposure to pure dry nitrogen as the baseline and to pure dry nitrogen (95%) plus H_2 (5%) as the target gas. a) Time-resolved XANES spectra at the Cu K-edge; b) electrical resistance over time; c) copper fraction species over time and d) first derivative of Cu the K-edge XANES spectra at different times.

The observed reduction kinetics were very similar for the measurements performed at different temperatures, as shown in Figure S3 and S4 in ESI†, indicating that the reduction process follows the same reaction kinetics but that the reaction rate slows with as the temperature decreases. We observed that, during the reduction process at higher temperatures, a huge increase in the concentration of Cu^+ species occurred, followed by a decrease and stabilization of the Cu^+ concentration over a very short period of time (less than 150 s at 400 °C and 300 s at 300 °C). By contrast, the concentration of Cu^0 species increased, as soon as the concentration of Cu^+ species decreased, followed by stabilization of those species. On the other hand, at 200 °C only a small fraction of Cu^{2+} species was reduced to Cu^+ species, and no Cu^0 species were observed in the quantification data. However, electrical resistance increased, followed by a decrease and stabilization, for a long period of exposure time, and then decreased again abruptly to low resistance values indicating metallic behavior. XANES is well-known to be a bulk technique, with limitations to detect small quantities of chemical species at the surface.[49] Thus, this result confirms that as expected, the reduction process occurs from the surface to the core of the urchin-like CuO nanostructures, which can perfectly explain why no metallic copper species

were detected at 200 °C in the XANES spectra but were able to be detected in the electrical measurements, i.e., a thin percolating layer of metallic copper at the surface of the urchin-like CuO nanostructures, at quantities undetectable by XANES, is sufficient to generate a change in sample conductivity because electrons will always flow through the pathway of lowest resistance. In addition, as soon as the formation of Cu^+ species had been begun a decreasing in resistance was noted. So, it could be expected that, in presence of oxygen, if a thin layer of Cu_2O was formed at the surface of the urchin-like CuO nanostructures, at quantities undetectable by XANES, a decreased resistance should be observed, similar to those observed at 200 °C in absence of oxygen, which was not (see Figure 1). This result may confirm that the main mechanisms, in presence oxygen, are those ones proposed by ionsorption model.[45,47] These results were possible only because the sample holder layout developed in this work provided XANES and electrical information concomitantly, thus allowing us to extract more details of the kinetic reaction due to the complementarity of the techniques in real time.

The mechanisms for CuO reduction involve an induction period followed by the diffusion of hydrogen into the solid bulk.[40,50] Our results indicate that the magnitude of the induction period is shorter at higher temperatures when, during the induction period, active sites are formed by the rapid dissociation of H_2 (Eq. 1).[18] Then, due to the absence of oxygen, the adsorbed hydrogen diffuses into the solid bulk, leading to the removal of lattice oxygen and forming water being faster at higher temperatures, according to Eq. 4 and 5.[50] Thus, based on our results, we believe that the copper reduction mechanism is likely one in which the Cu^{2+} species is reduced to Cu^+ species and then to Cu^0 species by reacting with adsorbed hydrogen chemical species, which may indicate the following sequence of reduction: $CuO \rightarrow Cu_2O \rightarrow Cu$. We believe that in the presence of hydrogen at isothermal conditions, Cu_2O is an intermediate unstable phase that appears only as a crystalline transient phase during the CuO reduction process, corroborating the results observed by Frenkel et al.[50] The reduction of copper changes the surface solid characteristics initially from those of CuO to those of Cu_2O and then to a Cu metal. This process occurs from the surface inward to the solid bulk when hydrogen is available, and the rate of reaction is temperature-dependent.

$$H^+_{(ads)} + CuO_{(s)} \rightarrow \tfrac{1}{2}\, Cu_2O_{(s)} + \tfrac{1}{2}\, H_2O_{(g)} \quad (4)$$
$$H^+_{(ads)} + \tfrac{1}{2}\, Cu_2O_{(s)} \rightarrow Cu_{(s)} + \tfrac{1}{2}\, H_2O_{(g)} \quad (5)$$

In Figure 3a, after 500 s, we can observe that the hydrogen was removed after the nitrogen baseline gas was reintroduced, but the sample maintained its high reduced copper fractions and low electrical resistance values, which was expected due to the absence of oxygen to induce copper oxidation (the same behavior was observed at different temperatures). To investigate the oxidation process and the gas sensor properties after oxidation, the sample was exposed to an oxidizing atmosphere by the injection of synthetic dry air to recover the sensor, as shown in Figure 3. At approximately 780 s, the sample was oxidized returning to its initial concentration of Cu^{2+} (80±3%) and Cu^+ (20±10%) species, and, consequently, the sensor resistance exhibited an abrupt increase resulting from the oxidation process. Finally, at approximately 1500 s, an increase in the electrical resistance was noted again when the nitrogen atmosphere was reintroduced and used until the end of the experiment (2250 s), confirming that the sensor returned to functioning as a p-type semiconductor. The first derivatives of the XANES spectra were calculated during sensor analysis at different times, as shown in Figure 3d, and clearly indicate the oxidation reaction kinetics at all stages of the measurements. Compared with the CuO experimental spectra with copper patterns, we can observe that the experimental spectra is very similar to the CuO spectra in the beginning and end of the measurement period, but, by contrast, the presence of metallic copper and Cu_2O can be clearly identified during the middle of the experiment. In addition, we can also observe from the quantification data that the copper oxidation at 400 °C occurred by two simultaneous processes, i.e., the metallic copper fraction was directly oxidized to Cu^{2+} without the formation of an intermediate phase, as indicated by the lack of increase in the concentration of Cu^+ species, and the same process occurred with the Cu^+ species oxidizing directly to Cu^{2+}, according to Equation 6 and 7. However, the oxidation process at lower temperatures (see Figure S4) followed different oxidation kinetics, with the copper metallic being quickly converted into Cu^+ species (Eq. 8) with a very short induction time and then slowly becoming Cu^{2+} species (Equation 7). These results indicate that the oxidation process is temperature-dependent, in which, at higher temperatures, the system contains enough energy to activate both reactions concomitantly, whereas at lower temperatures, the system follows the step-by-step oxidation sequence, which demands lower energy and a longer reaction time.[40]

$$\tfrac{1}{2}O_{2(g)} + Cu_{(s)} \rightarrow CuO_{(s)} \quad (6)$$
$$\tfrac{1}{2}\, O_{2(g)} + Cu_2O_{(s)} \rightarrow 2CuO_{(s)} \quad (7)$$
$$\tfrac{1}{2}O_{2(g)} + 2Cu_{(s)} \rightarrow Cu_2O_{(s)} \quad (8)$$

We have demonstrated in our previous work that urchin-like CuO nanostructures maintained their morphological characteristics after gas sensor measurements at different temperatures and atmospheres, which indicated the lack of structural/electronic alterations, as confirmed in this work.[18] Here, we performed an *ex situ* morphological study to analyze the morphology evolution during the reduction/oxidation process. The FESEM images from the *ex situ* morphological study of the urchin-like CuO nanostructures are shown in Figure 4. Figure 4a shows the as-prepared CuO sample, which exhibits a morphology similar to that of sea urchins, with a solid core covered by nanometric spines. For further characterizations and details of this sample, see our previous works.[18,39] However, after the sample was exposed to hydrogen at 400 °C, we observed the dissolution of the spines in the initial CuO morphology due to the reduction process, as

observed in Figure 4b, but the core structure remained. Finally, investigate morphological changes after oxidation, the sample was exposed to synthetic dry air at 400 °C, as shown in Figure 4c. The image suggests that the initial urchin-like morphology was not rebuilt but rather that a new structure was generated where the cores remained, with a growth of microparticles distributed around the whole surface. Energy dispersive X-ray (EDX) analysis was performed for each step of oxidation and reduction, as shown in Figure S5 in ESI†, in which the presence of Cu and O were confirmed, but at different concentration for oxidized and reduced conditions. So, the morphological, EDX and XANES results may provide an explanation as to why the sample maintained a determined concentration of different copper species during the reduction/oxidation processes, i.e., the reduction process occurs mainly at the surface, and potentially in the first layers of the solid core, but, due to its higher density, the hydrogen did not diffuse into the solid core, thus leaving a certain concentration of different copper species inside the core, with similar mechanisms occurring during the oxidation process.

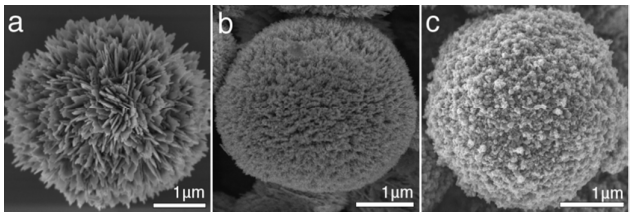

Figure 4. FESEM images of the CuO samples. a) As-prepared urchin-like structures, b) after reduction and c) after oxidation.

Conclusions

In summary, a systematic examination of the structural, electronic and electrical characteristics of an urchin-like CuO nanostructured semiconductor material exposed to reducing gas under different baseline gases over a range of temperatures were analyzed in real time using *in situ* XANES and electrical measurements simultaneously in the same test chamber. The conception of our sample holder layout resulted in high-precision XANES spectra, which was very important for the semi-quantitative analyses; low-noise electrical measurements and very precise and effective correlations between the XANES and electrical data. This sample holder will facilitate the realization of future studies by the simultaneous acquisition of time-resolved data with electrical measurements for a wide range of materials for applications such as fuel cells, electro- and photochemical devices, among others. Our results indicate that CuO is highly unstable under high reducing atmospheres and temperatures, under which the gas sensor behavior or reduction process is controlled by the presence of an oxygen atmosphere. Gas sensor behavior is mainly related to the induction/absence of electron/holes at the CuO surface, resulting in conductivity changes due to solid-gas interactions. On the other hand, reduction/oxidation processes are more complex mechanisms that are highly influenced by the temperature, as a consequence of the interactions between the absorbed chemical species and the lattice cations, which serve as a conduit for conductivity changing arising from the solid phase transition. Before one can affirm whether the use of CuO semiconductor oxides as active element in gas sensor devices may be restricted to the air atmosphere conditions, additional studies, which are already in process, must be performed to deconvolute the limit of the oxygen partial pressure required to prevent copper reduction. main text of the article should appear here with headings as appropriate..

Acknowledgements

D.P. Volanti and A.A. Felix contributed equally to this work. The authors acknowledge the São Paulo Research Foundation (FAPESP) (Proc. 13/07296-2, Proc. 13/14647-6, and Proc. 11/02408-1). The XANES facilities in this work were provided by LNLS-CNPEM (National Laboratory of Synchrotron Light, Brazil) at the beamline D06A-DXAS under the proposal numbers 13710, 12584, and 11845. The authors thank the LNNano/LME and GAE-LNLS staff for their support and help the in microfabrication process. We express our gratitude to Narcizo M. Souza-Neto, Alexey Spindola, Fabio Zambello, and Anna Paula da Silva Sotero Levinsky for useful instrumental setup contributions.

Notes and references

1. Y. Wang, B. Liu, S. Xiao, H. Li, L. Wang, D. Cai, D. Wang, Y. Liu, Q. Li and T. Wang, *J. Mater. Chem. A*, 2015, **3**, 1317.
2. D. Hu, B. Han, S. Deng, Z. Feng, Y. Wang, J. Popovic, M. Nuskol, Y. Wang and I. Djerdj, *J. Phys. Chem. C*, 2014, **118**, 9832.
3. I.-D. Kim, A. Rothschild and H. L. Tuller, *Acta Mater.*, 2013, **61**, 974.
4. D.-J. Yang, I. Kamienchick, D. Y. Youn, A. Rothschild, I.-D. Kim, Adv. Funct. Mater. 2010, **20**, 4258.
5. X. Zhou, S. Lee, Z. Xu and J. Yoon, *Chem. Rev.*, 2015, DOI: 10.1021/cr500567r.
6. H.-J. Kim and J.-H. Lee, *Sens. Actuators, B*, 2014, **192**, 607.
7. L. Yu, Y. Huang, G. Xiao and D. Li, *J. Mater. Chem. A*, 2013, **1**, 9637.
8. J. Du, Z. Chen, S. Ye, B. J. Wiley and T. J. Meyer, *Angew. Chem. Int. Ed.*, 2015, **54**, 2073.
9. S. Maddila, S. Rana, R. Pagadala, S. Kankala, S. Maddila and S. B. Jonnalagadda, *Catal. Commun.*, 2015, **61**, 26.
10. W.-W. Wang, P.-P. Du, S.-H. Zou, H.-Y. He, R.-X. Wang, Z. Jin, S. Shi, Y.-Y. Huang, R. Si, Q.-S. Song, C.-J. Jia and C.-H. Yan, *ACS Catalysis*, 2015, **5**, 2088.
11. A. A. Pechenkin, S. D. Badmaev, V. D. Belyaev and V. A. Sobyanin, *Appl. Catal., B*, 2015, **166**, 535.
12. R. L. Z. Hoye, R. E. Brandt, Y. Ievskaya, S. Heffernan, K. P. Musselman, T. Buonassisi and J. L. MacManus-Driscoll, *APL Mater.*, 2015, **3**, 020901.
13. J. Zhang, J. Wang, Y. Fu, B. Zhang and Z. Xie, *RSC Adv.*, 2015, **5**, 28786.

14. X.-Y. Yu, R.-X. Xu, C. Gao, T. Luo, Y. Jia, J.-H. Liu and X.-J. Huang, *ACS Appl. Mater. Interfaces*, 2012, **4**, 1954.
15. Q. Zhang, K. Zhang, D. Xu, G. Yang, H. Huang, F. Nie, C. Liu and S. Yang, *Prog. Mater Sci.*, 2014, **60**, 208.
16. J. Y. Xiang, J. P. Tu, L. Zhang, Y. Zhou, X. L. Wang and S. J. Shi, *J. Power Sources*, 2010, **195**, 313.
17. S. Manna, K. Das and S. K. De, *ACS Appl. Mater. Interfaces*, 2010, **2**, 1536.
18. D. P. Volanti, A. A. Felix, M. O. Orlandi, G. Whitfield, D.-J. Yang, E. Longo, H. L. Tuller and J. A. Varela, *Adv. Funct. Mater.*, 2013, **23**, 1759.
19. C. Wang, J. Zhu, S. Liang, H. Bi, Q. Han, X. Liu and X. Wang, *J. Mater. Chem. A*, 2014, **2**, 18635.
20. Q. Simon, D. Barreca, A. Gasparotto, C. Maccato, E. Tondello, C. Sada, E. Comini, G. Sberveglieri, M. Banerjee, K. Xu, A. Devi and R. A. Fischer, *ChemPhysChem*, 2012, **13**, 2342.
21. M. M. Rahman, A. Jamal, S. B. Khan and M. Faisal, *ACS Appl. Mater. Interfaces*, 2011, **3**, 1346.
22. J. J. Benítez, M. A. Centeno, C. L. dit Picard, O. Merdrignac, Y. Laurent and J. A. Odriozola, *Sens. Actuators, B*, 1996, **31**, 197.
23. A. Gurlo and R. Riedel, *Angew. Chem. Int. Ed.*, 2007, **46**, 3826.
24. A. Gurlo and R. Riedel, *ChemPhysChem*, 2010, **11**, 79.
25. Z. Zhang, K. Huang, F. Yuan and C. Xie, *Appl. Surf. Sci.*, 2014, **300**, 98.
26. M. Hübner, C. E. Simion, A. Tomescu-Stănoiu, S. Pokhrel, N. Bârsan and U. Weimar, *Sens. Actuators, B*, 2011, **153**, 347.
27. K. Grossmann, R. G. Pavelko, N. Barsan and U. Weimar, *Sens. Actuators, B*, 2012, **166**, 787.
28. H.-R. Kim, A. Haensch, I.-D. Kim, N. Barsan, U. Weimar and J.-H. Lee, *Adv. Funct. Mater.*, 2011, **21**, 4456.
29. K. Grossmann, N. Barsan and U. Weimar, *Eurosensors XXIV Conference*, 2010, **5**, 119.
30. J. Zhong, H. Zhang, X. Sun and S.-T. Lee, *Adv. Mater.*, 2014, **26**, 7786.
31. F. J. Garcia-Garcia, J. Gil-Rostra, F. Yubero, J. P. Espinós, A. R. Gonzalez-Elipe and J. Chaboy, *J. Phys. Chem. C*, 2014, **119**, 644.
32. D. Buchholz, J. Li, S. Passerini, G. Aquilanti, D. Wang and M. Giorgetti, *ChemElectroChem*, 2015, **2**, 85.
33. C. N. Ávila-Neto, J. W. C. Liberatori, A. M. da Silva, D. Zanchet, C. E. Hori, F. B. Noronha and J. M. C. Bueno, *J. Catal.*, 2012, **287**, 124.
34. W.-Q. Shi, L.-Y. Yuan, C.-Z. Wang, L. Wang, L. Mei, C.-L. Xiao, L. Zhang, Z.-J. Li, Y.-L. Zhao and Z.-F. Chai, *Adv. Mater.*, 2014, **26**, 7807.
35. M. Hüebner, D. Koziej, J.-D. Grunwaldt, U. Weimar and N. Barsan, *PCCP*, 2012, **14**, 13249.
36. J.-D. Grunwaldt, M. Huebner, D. Koziej, N. Barsan and U. Weimar, *Journal of Physics Conference Series*, 2013, **430**, 012078.
37. M. Hüebner, D. Koziej, M. Bauer, N. Barsan, K. Kvashnina, M. D. Rossell, U. Weimar and J.-D. Grunwaldt, *Angew. Chem. Int. Ed.*, 2011, **50**, 2841.
38. D. Koziej, M. Hubner, N. Barsan, U. Weimar, M. Sikora and J.-D. Grunwaldt, *PCCP*, 2009, **11**, 8620.
39. D. P. Volanti, A. G. Sato, M. O. Orlandi, J. M. C. Bueno, E. Longo and J. Andres, *ChemCatChem*, 2011, **3**, 839.
40. J. Y. Kim, J. A. Rodriguez, J. C. Hanson, A. I. Frenkel and P. L. Lee, *J. Am. Chem. Soc.*, 2003, **125**, 10684.
41. C. M. Chanquía, K. Sapag, E. Rodríguez-Castellón, E. R. Herrero and G. A. Eimer, *J. Phys. Chem. C*, 2010, **114**, 1481.
42. E. Moretti, M. Lenarda, L. Storaro, A. Talon, R. Frattini, S. Polizzi, E. Rodríguez-Castellón and A. Jiménez-López, *Appl. Catal., B*, 2007, **72**, 149.
43. A. Caballero, J. J. Morales, A. M. Cordon, J. P. Holgado, J. P. Espinos and A. R. Gonzalez-Elipe, *J. Catal.*, 2005, **235**, 295.
44. S. Velu, K. Suzuki, C. S. Gopinath, H. Yoshida and T. Hattori, *PCCP*, 2002, **4**, 1990.
45. N. Barsan, C. Simion, T. Heine, S. Pokhrel and U. Weimar, *J. Electroceram.*, 2010, **25**, 11.
46. A. Oprea, N. Bârsan and U. Weimar, *Sens. Actuators, B*, 2009, **142**, 470.
47. S. R. Morrison, *The Chemical Physics of Surfaces*, Plenum Press, 1977.
48. M. J. Madou and S. R. Morrison, *Chemical Sensing with Solid State Devices*, Academic Press, New York, 1989.
49. G. Bunker, *Introduction to XAFS - A Practical Guide to X-ray Absorption Fine Structure Spectroscopy*, Cambridge University Press, Cambridge, 1st edn., 2010.
50. J. A. Rodriguez, J. Y. Kim, J. C. Hanson, M. Perez and A. I. Frenkel, *Catal. Lett.*, 2003, **85**, 247.